Effect of gravity on clustering patterns and inertial particle attractors in kinematic simulations

M. Farhan, F. C. G. A. Nicolleau,* and A. F. Nowakowski

Sheffield Fluid Mechanics Group, Department of Mechanical Engineering, The University of Sheffield, Sheffield, United Kingdom

(Received 28 October 2014; revised manuscript received 13 February 2015; published 29 April 2015)

In this paper, we study the clustering of inertial particles using a periodic kinematic simulation. The systematic Lagrangian tracking of particles makes it possible to identify the particles' clustering patterns for different values of particle inertia and drift velocity. The different cases are characterized by different pairs of Stokes number (St) and Froude number (Fr). For the present study, $0 \leqslant \mathrm{St} \leqslant 1$ and $0.4 \leqslant \mathrm{Fr} \leqslant 1.4$. The main focus is to identify and then quantify the clustering attractor—when it exists—that is the set of points in the physical space where the particles settle when time goes to infinity. Depending on the gravity effect and inertia values, the Lagrangian attractor can have different dimensions, varying from the initial three-dimensional space to two-dimensional layers and one-dimensional attractors that can be shifted from a horizontal to a vertical position.

DOI: 10.1103/PhysRevE.91.043021 PACS number(s): 47.27.Gs, 47.55.Kf, 47.85.lk

I. INTRODUCTION

Clustering could be defined as the propensity of an initially uniformly distributed cloud of particles to accumulate in some regions of physical space. This is an important phenomenon to understand in order to explore, identify, and possibly monitor some natural or handmade mixing processes, such as those causing rain formation [1], sediment transportation [2], fuel mixing, and combustion.

There are different ways to analyze particle clustering in turbulent flow and direct numerical simulation (DNS) is the most widely used method (e.g., [3–5]). Particle clustering depends on both the flow conditions and the particle characteristics. Different flow conditions can lead to different clusters. The clustering mechanism would be different in the inertial or dissipation range of turbulent flow [6]. In our paper, we only study the effect of the scales in the inertial range and this is possible by using a synthetic model where forcing and dissipation are not needed to develop the inertial range. While considering particle characteristics, most of the studies on particle clustering have been conducted in the absence of external forces on particles, but the effect of gravity (external force) was discussed in relation to cloud physics and rain formation in [5,7].

More recently, the effect of gravity on the clustering mechanism has been further emphasized in [8–10]. In the present study, to observe the clustering pattern in the presence of gravity, the particles are initially uniformly distributed in the kinematic simulation (KS) flow. Though there is no particular difficulty in considering particles with different inertia in kinematic simulation, this study is limited to monodispersed seeding, i.e., particles having the same inertia. Furthermore, the particles are considered small enough so that they neither affect the flow nor interact with each other (one-way coupling). The positions of particles are monitored as a function of time and a Lagrangian attractor is observed for some cases. That is, the initially distributed cloud of particles will end in a set of loci that does not evolve any further. The particles move within that set of loci, which defines the structure of the Lagrangian attractor, and its dependence on St and Fr numbers is studied here.

We only consider attractors with integer dimensions (one-dimensional and two-dimensional structures) which are easy to identify. Different types of methods can be found in the literature to identify and then quantify particle clustering patterns, e.g., correlation dimension [6], radial distribution function (RDF) [4], and the average-distance-to-nearest-neighbor method [8]. The selection of a method is mainly based on the objective of the study. For example, the RDF has the advantage of being directly related to the droplet collision rate. For the present work, the box-counting method (BCM) and the nearest-neighbor-distance analysis are implemented to identify the integer dimensions of Lagrangian attractor in the presence of gravity.

The paper is organized as follows: in Sec. II, we introduce the KS model, its notations, and its parameters. The different kinds of Lagrangian attractor are discussed and introduced in Sec. III. A quantitative analysis is conducted in Sec. IV. Section V summarizes our main conclusions.

II. KINEMATIC SIMULATION TECHNIQUE

Kinematic simulation (KS) is a particular case of synthetic turbulence where the focus is on the particle's trajectory at the expense of solving the Navier-Stokes equation. An analytical formula "synthetic flow" is used for the Eulerian flow field. The simplicity of the KS model excludes some features of real turbulent flow, but captures the part of the physics which is required to perform Lagrangian particle tracking. Such is the idea with synthetic turbulence, which retains less information than the whole flow, but tries to keep what is paramount for the Lagrangian story.

KS modeling has been successfully employed and validated [11–13]. This kind of simulation is much less consuming of computing time than DNS which is important for the present study where we need to run many cases (about 400 cases for up to 1200 turnover time). Each case corresponds to a given St, Fr, and time and involves 15 625 particles.

With synthetic simulations, one can develop models where turbulence ingredients and complexity can be added step by step, helping researchers to understand their respective

*Corresponding author: F.Nicolleau@Sheffield.ac.uk

importance. These synthetic models can be a useful complement to direct numerical simulation. In particular, KS was instrumental in discriminating between the role of Lagrangian and Eulerian correlations for vertical diffusion in stratified and rotating flows [14]. With KS, it is also possible to play with the spectral law [15] and its consequences in terms of the particle's dispersion. We also refer to the work of [16,17] for a discussion of how the work on KS can help to understand the sweeping effect on two-particle dispersion.

KS was first introduced as a way to understand particle dispersion rather than particle clustering, but we propose here a work getting back to the main strength of KS, which is to provide a coherent Lagrangian framework where some parameters (e.g., spectra [15], waves [14,18], etc.) can be studied in detail, posing the basis for a comparison with experiments. Previous work [19,20] particularly supports the use of KS for studying the evolution of the particle cloud in the absence of gravity effect, which made the study more about segregation than clustering.

As we are not interested in two-particle dispersion, we limit our study to small Reynolds numbers, more precisely, to scale ratio $k_{i\,\max}/k_{i\,\min} = 15$ ($i = 1$, 2, or 3).

A. Periodic KS method for isotropic turbulence

In kinematic simulation, the underlying Eulerian velocity field is generated as a sum of random incompressible Fourier modes with a prescribed energy spectrum $E(k)$. Here we limit the study to a Kolmogorov-type spectral law, $E(k) \sim k^{-5/3}$. Using KS, the computational task reduces to calculate the trajectory of each particle placed in the turbulent field initially at $\mathbf{X}_0$. Each trajectory is, for a given initial condition, a solution of the differential equation set

$$\frac{d\mathbf{X}}{dt} = \mathbf{V}(t), \tag{1}$$

$$\frac{d\mathbf{V}}{dt} = \mathfrak{F}[\mathbf{u}_E(\mathbf{X},t),\mathbf{V},t], \tag{2}$$

where $\mathbf{X}(t)$ is the particle's position, $\mathbf{V}(t)$ is its Lagrangian velocity, and $\mathbf{u}_E$ is the analytical Eulerian velocity used in KS. $\mathfrak{F}$ is a function relating the Lagrangian acceleration to the Eulerian and Lagrangian velocities.

In KS, $\mathbf{u}_E$ takes the form of a truncated Fourier series, i.e., the sum of $N_k = N^3$ Fourier modes:

$$\mathbf{u}(\mathbf{x}) = \sum_{i=1}^{N}\sum_{j=1}^{N}\sum_{K=1}^{N} \mathbf{a_{ijl}}\cos(\mathbf{k_{ijl}}\cdot\mathbf{x}) + \mathbf{b_{ijl}}\sin(\mathbf{k_{ijl}}\cdot\mathbf{x}), \tag{3}$$

where $\mathbf{a_{ijl}}$ and $\mathbf{b_{ijl}}$ are the decomposition coefficients corresponding to the wave vector $\mathbf{k_{ijl}}$. In its general form, the KS field can also be a function of time, but we limit the study to a steady KS. The effect of introducing a time dependence in the Fourier modes will be the objective of future study.

Unlike the classic KS decomposition [21,22], here the wave vectors $\mathbf{k_{ijl}} = (k_i,k_j,k_l)$ are implemented arithmetically to enforce a periodic condition for the flow field:

$$k_i = \frac{2\pi}{L_x}(n_i - 1), \tag{4}$$

$$k_j = \frac{2\pi}{L_y}(n_j - 1), \tag{5}$$

$$k_l = \frac{2\pi}{L_z}(n_l - 1), \tag{6}$$

where (n_i,n_j,n_k) are integers satisfying $1 \leqslant n_i \leqslant N$. In practice, we choose $(L_x = L_y = L_z)$ for creating isotropic turbulence and to ensure the flow incompressibility; the Fourier coefficient vectors $\mathbf{a_{ijl}}$ and $\mathbf{b_{ijl}}$ are set orthogonal to the wave vector,

$$\mathbf{a_{ijl}}\cdot\mathbf{k_{ijl}} = \mathbf{b_{ijl}}\cdot\mathbf{k_{ijl}} = 0. \tag{7}$$

Their magnitude is fixed by the energy spectrum, $E(k)$,

$$|\mathbf{a_{ijk}}|^2 = |\mathbf{b_{ijk}}|^2 = 2E(k)\Delta k_{ijl}/m_k, \tag{8}$$

where m_k is the number of wave vectors of wave number $k = \|\mathbf{k_{ijl}}\|$. The spectrum follows the Kolmogorov form in the inertial range,

$$E(k) = A\,k^{-5/3} \quad \text{for} \quad k_{\min} \leqslant k \leqslant k_{\max}, \tag{9}$$

where A is a constant. From the spectral law, the rms velocity and the integral length scale can be defined as follows:

$$u_{\rm rms} = \sqrt{\frac{2}{3}\int_{k_{\min}}^{k_{\max}} E(k)dk}, \tag{10}$$

$$\mathcal{L} = \frac{3\pi}{4}\frac{\int_{k_{\min}}^{k_{\max}} k^{-1}E(k)dk}{\int_{k_{\min}}^{k_{\max}} E(k)dk}. \tag{11}$$

The Kolmogorov length scale is defined as $\eta = 2\pi/k_{\max}$, whereas the largest physical scale is $L = 2\pi/k_{\min}$, which determines the inertial range $[\eta,L]$ over which (9) is observed. It is worth noting that $\mathcal{L} \simeq L$ for sufficiently large inertial ranges. However, here in contrast to other KS studies the inertial range is small and $L \simeq 5\mathcal{L}$. In this paper, nondimensional numbers (St and Fr) are based on the integral length scale $\mathcal{L}$ and, for the sake of future comparisons, both are reported in Table I. The ratio between the largest length scale and the Kolmogorov length scale is $k_{\max}/k_{\min}$ and the associated Reynolds number

TABLE I. Periodic KS parameters.

$L_x = L_y = L_z$	1
N	10
N_p	15625
$u_{\rm rms}$	0.8703
$\mathcal{L}$	0.2106
L	1
η	0.0642
$\mathcal{T}$	0.2420
t_d	1.1491
$k_i/k_{i\,\min}$	15
$k_{\max}/k_{\min}$	15.5885
Re_L	38.94

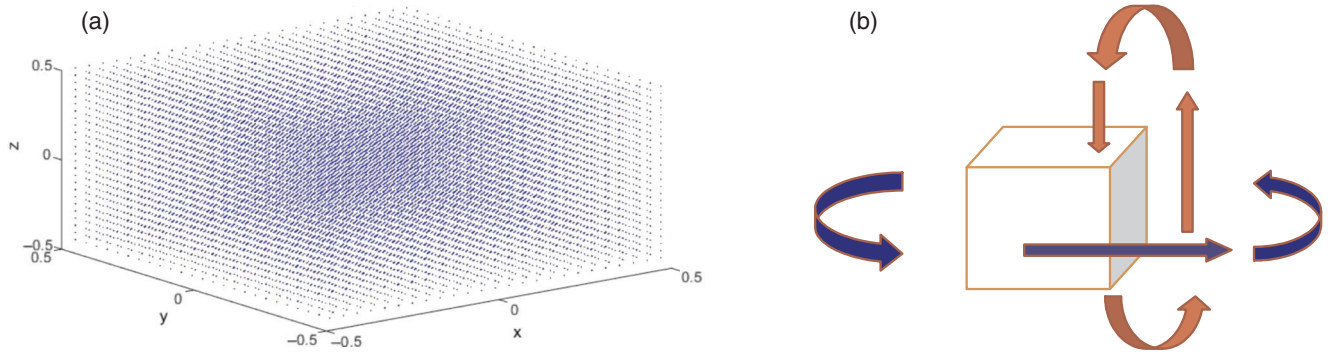

FIG. 1. (Color online) Particles' (a) initial distribution and (b) reinjection.

is $\mathrm{Re}_L = (k_{\max}/k_{\min})^{4/3}$. This is the standard way to define a Reynolds number in KS, and a DNS or an experiment yielding the same ratio $k_{\max}/k_{\min}$ would have a much larger Reynolds number. Finally, a characteristic time for normalization can be $t_d = L/u_{\mathrm{rms}}$ or $\mathcal{T} = \mathcal{L}/u_{\mathrm{rms}}$. All of the periodic KS parameters are gathered in Table I.

The particles are initially homogeneously distributed, as shown in Fig. 1(a), and whenever a particle leaves the turbulence box domain (e.g., $\mathbf{X}_i > L_x$), it is reinjected from the opposite side, as shown in Fig. 1(b), to keep the periodic condition.

B. Equation of motion

Following [23], the equation of motion for the inertial particle is derived from [24,25] and consists of a drag force and drift acceleration (weight),

$$\frac{d\mathbf{V}}{dt} = \frac{1}{\tau_a}\{\mathbf{u}[\mathbf{x}_p(t),t] - \mathbf{V}(t) + \mathbf{V}_d\}, \tag{12}$$

where τ_a is the particle's aerodynamic response time and $V_d = \tau_a\,\mathbf{g}$ is the particle's terminal fall velocity or drift velocity.

C. Nondimensional parameters

Three nondimensional parameters are introduced to make qualitative and quantitative analyses of the particle clustering.

(a) The Stokes number expresses the ratio between the particle's response time (inertia effect) and the turbulence characteristic time,

$$\mathrm{St} = \tau_a/\mathcal{T} = \tau_a u_{\mathrm{rms}}/\mathcal{L}. \tag{13}$$

It measures the relative importance of the particle inertia. In the limiting case $\mathrm{St} = 0$, the heavy particles recover the motion of the fluid tracers, whereas for $\mathrm{St} \to \infty$, the heavy particles become less and less influenced by the surrounding velocity field.

(b) The Froude number is the ratio between inertial forces and gravitational forces,

$$\mathrm{Fr} = u_{\mathrm{rms}}/\sqrt{g\mathcal{L}}. \tag{14}$$

In our study, the rms velocity u_{rms} and inertial length scale are constant and g is varied.

(c) The drift parameter is the ratio between the particle's drift velocity and the turbulence rms velocity,

$$\gamma = V_d/u_{\mathrm{rms}}. \tag{15}$$

The drift parameter can still be defined without gravity. Then γ can be considered as measuring the effect of a mean velocity V_d.

If V_d is caused by gravity,

$$\gamma = \tau_a g/u_{\mathrm{rms}}, \tag{16}$$

then in this case the drift parameter is affected by both the gravity and the particle's inertia.

(d) γ can be expressed as a function of Stokes and Froude numbers so, for a given turbulence, the case corresponding to a constant gravity, that is, varying τ_a only, is given by

$$\mathrm{Fr} = \mathrm{const}, \tag{17}$$

$$\gamma \sim \mathrm{St}. \tag{18}$$

III. RESULTS AND DISCUSSION

A. Clustering pattern variations in relation to time of evolution

The particles initially uniformly distributed in the flow field are allowed to evolve until a Lagrangian attractor is achieved. The shape of the attractor varies from clear one-dimensional structures (Figs. 2 and 3) to three-dimensional distributed structures column (d) of Fig. 4(e) or two-dimensional curtain-like structures [column (d) of Fig. 4(h)]. For a short time, the attractor's shape is time dependent, as shown in Figs. 2 and 3. The time evolution of the cluster depends on nondimensional parameters St and Fr, as illustrated in Fig. 2, where it takes four times longer to reach the one-dimensional Lagrangian attractor than in the case of Fig. 3. In this paper, we do not intend to study the temporal evolution of cluster attractors and are only interested in the attractor's asymptotic form (i.e., for $t \to \infty$).

In this section, we focus on the qualitative measure of attractors and only a few cases are presented in Figs. 4 and 5. A systematic quantification will be proposed in Sec. IV, which consists of a comprehensive set of data generated with small increments in Fr and St numbers. As the one-dimensional Lagrangian attractor is observed for various pairs of St and

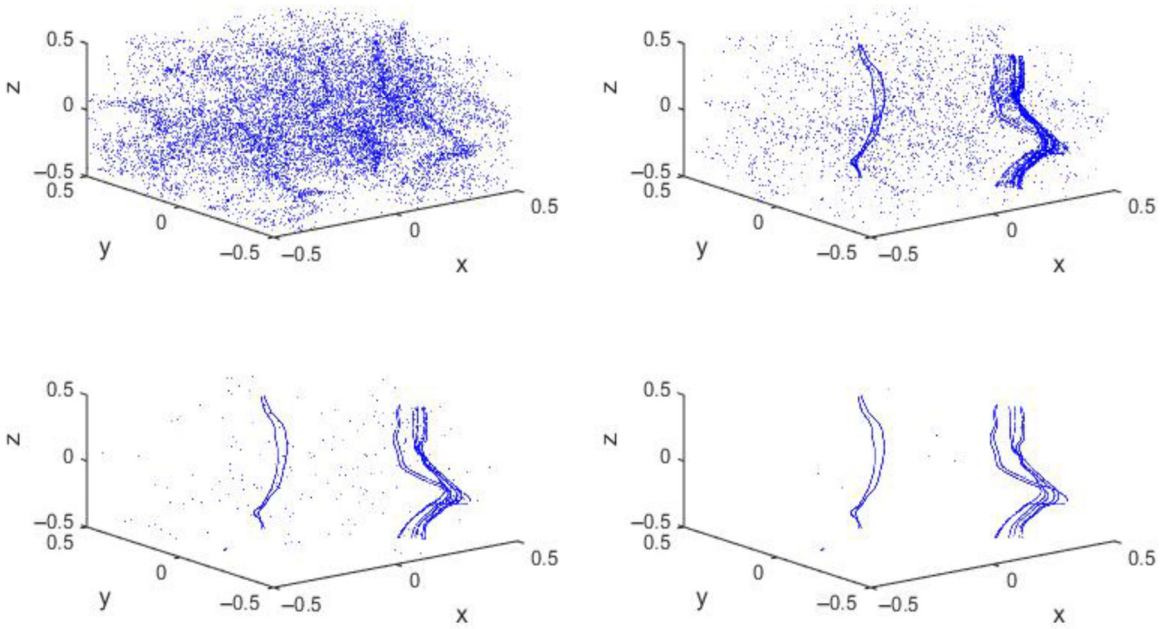

FIG. 2. (Color online) Time evolution of inertial particles for St = 0.207 and Fr = 0.55 with $t = 1$ (top left), $t = 10$ (top right), $t = 600$ (bottom left), and $t = 1200$ (bottom right).

Fr, it was difficult to suggest any definite relationship between one-dimensional clustering and St and Fr. Hence, a scheme of further classification is adopted to establish such a relationship. We use the following nomenclature:

(i) 1D-H: horizontal one-dimensional Lagrangian attractor as in column (b) of Fig. 4(f).

(ii) 1D-V: vertical one-dimensional Lagrangian attractor as in column (b) of Fig. 4(g).

(iii) 1D-HV: intermediate one-dimensional Lagrangian attractor as in columns (a) and (c) of Fig. 4(g).

(iv) 2D-L: two-dimensional vertical curtainlike layer as in column (d) of Fig. 4(h) (see also [7]).

(v) 3D: any three-dimensional structure without any particular structure in the cloud as in column (d) of Fig. 4(e).

The qualitative results are split into three different categories which can take into account the effect of gravity and/or inertia:

(i) keeping St constant (Sec. III B),

(ii) keeping Fr constant (Sec. III C),

(iii) keeping γ constant (Sec. III D).

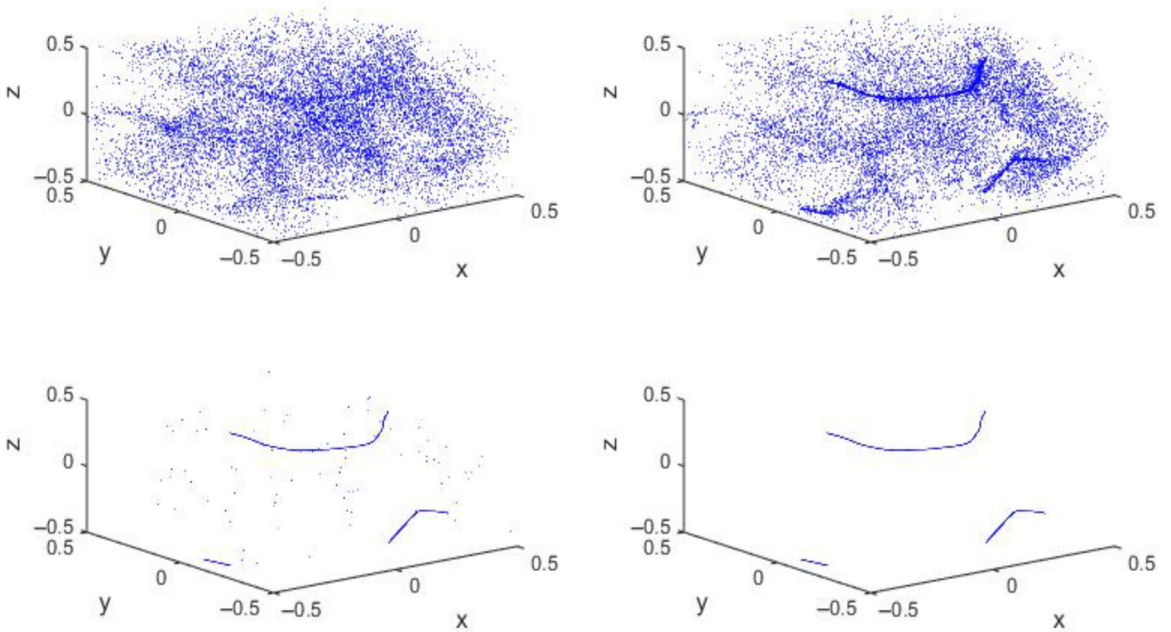

FIG. 3. (Color online) Time evolution of inertial particles for St = 0.413 and Fr = 0.85 with $t = 1$ (top left), $t = 5$ (top right), $t = 100$ (bottom left), and $t = 300$ (bottom right).

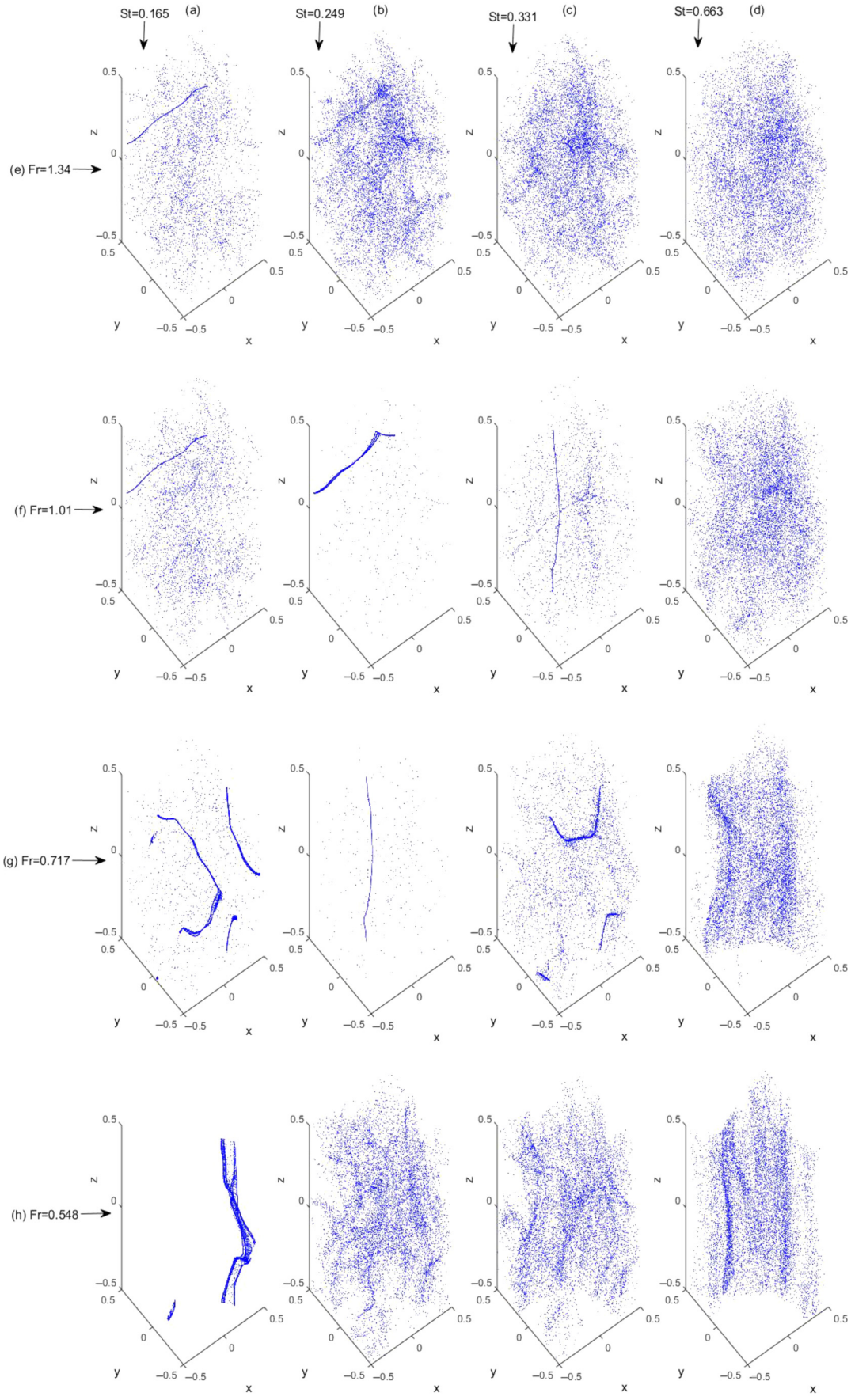

FIG. 4. (Color online) Evolution of the particles cloud for $0.548 \leqslant \mathrm{Fr} \leqslant 1.34$ and $0.165 \leqslant \mathrm{St} \leqslant 0.663$, at $t = 300$.

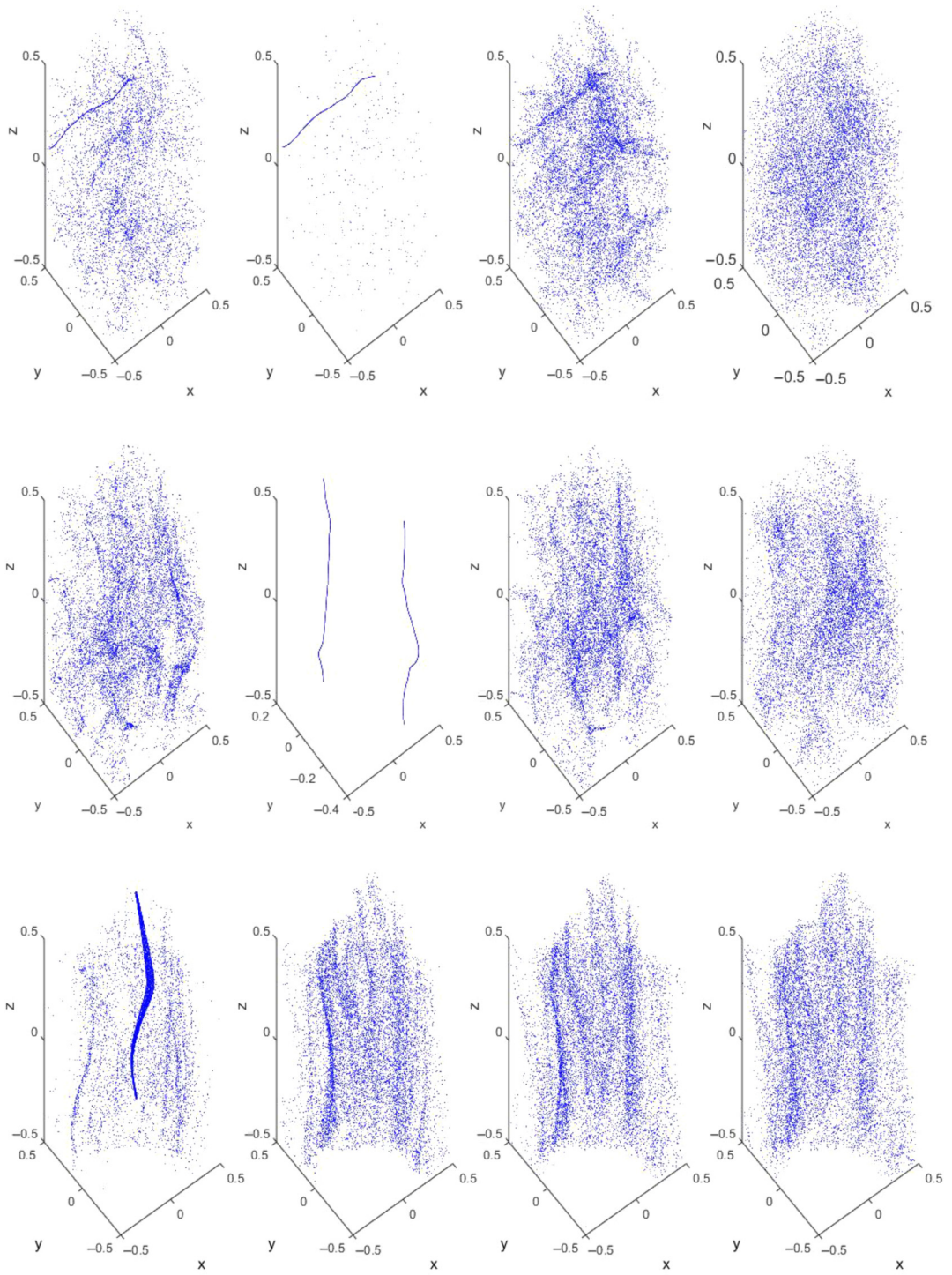

FIG. 5. (Color online) Evolution of particles with increasing St for a given γ at $t = 300$. Top: $\gamma = 0.138$; left to right: St = 0.100, 0.165, 0.249, and 1. Middle: $\gamma = 0.689$; left to right: St = 0.124, 0.165, 0.249, and 0.827. Bottom: $\gamma = 2$; left to right: St = 0.207, 0.600, 0.827, and 1.

B. Clustering pattern variations in relation to constant Stokes number (St)

We can analyze the results by fixing the Stokes number (St) and varying the Froude number (Fr). Four representative cases with varying values of Fr are shown in Figs. 4(a)–4(d), namely, St = 0.165, 0.249, 0.331, and 0.663. For each of the Stokes numbers, we explored within the range $0.548 \leqslant \mathrm{Fr} \leqslant 1.34$.

As the Froude number decreases, the particles first cluster on a one-dimensional Lagrangian attractor; then they may rearrange on another 1D or 2D Lagrangian attractor columns (b) and (c) of Fig. 4(h), and column (d) of Figs. 4(g) and 4(h). The Lagrangian attractor also moves from a predominantly horizontal direction [column (a) of Fig. 4(e) and columns (a) and (b) of Fig. 4(f)] to a vertical direction [columns (a) and (b)

TABLE II. Different cases for studying the attractor topology for different ranges of St.

			Observed patterns			
Case	St range	Fr range	1D-H	1D-V	2D-L	3D
A	0.041–0.124	0.42–1.34	√			√
B	0.165–0.300	0.42–1.34	√	√		√
C	0.331–0.413	0.42–1.34		√	√	√
D	0.496–1.000	0.42–1.34			√	√

TABLE III. Different cases for studying the attractor topology for different ranges of Fr.

			Observed patterns			
Case	Fr	St range	1D-H	1D-V	2D-L	3D
E	1.01	0–1	√	√		√
F	0.717	0–1		√	√	√
G	0.548	0–1		√	√	

of Fig. 4(g) and column (c) of Fig. 4(f)] with decreasing value of Fr.

The qualitative shapes with varying values of Fr are listed in Table II. When one-dimensional structures are in-between horizontal and vertical (1D-HV) directions, as in column (b) of Fig. 4(f), we ticked both 1D-H and 1D-V in the table.

Now we describe each case one by one according to observed patterns. For case A, corresponding to low values of St, the decrease in Fr (increase in gravity) forces the particles to cluster in a horizontal direction, whereas the particles will disperse evenly as Fr is further decreased. The increases in gravity destroy the particles' clustering for low range of St. Similarly, for case B, initially distributed inertial particles cluster into a horizontal attractor (1D-H), as in column (b) of Fig. 4(f), and then an increase in the gravity effect (lower Fr) causes the particles to accumulate in the vertical direction (1D-V), as in column (b) of Fig. 4(g). With further increases in the gravity, they recover a 3D distribution, as shown in column (b) of Fig. 4(h).The appearance of 1D-V in case B shows the greater effectiveness of gravity at a relatively high range of the St for a given value of Fr.

For further increases in the Stokes number St (case C), the horizontal structure (1D-H) is not observed. Rather a vertical 1D pattern (1D-V) is seen, as in column (c) of Fig. 4(f), which can transform into a 1D-HV attractor, as in column (c) of Fig. 4(g), with decreasing values of Fr. This implies that the particle inertia starts dominating over the flow Eulerian structure and allows the gravity to play a more important role. At higher values of St (case D), there is no more one-dimensional clustering, but some clustering can still be observed in the form of two-dimensional vertical curtainlike structures, as shown in column (d) of Fig. 4(h), at low values of Fr.

C. Clustering pattern variations in relation to constant Froude number (Fr)

A constant Froude number corresponds to the case of varying the particle's property (τ_a) for a given environment (turbulence and gravity), which exists in most of the experimental situations. The variations in clustering patterns are identified by keeping Fr constant while varying St. For the purpose of qualitative measures, three different cases, as shown in Table III, are considered with small increments in the St ranging from 0 to 1.

In Fig. 4, cases of constant Fr correspond to the horizontal rows [Figs. 4(e)–4(h)]. As St increases, the particles' one-dimensional clustering is first enhanced and then destroyed to eventually reappear in the form of a two-dimensional layer (2D-L).

For high values of Fr (low gravity), i.e., case E corresponding to Fig. 4(f), particles settled on horizontal one-dimensional structures (1D-H) for low values of St. The increase in St values resulted in vertical one-dimensional structures (1D-V). For the midrange values of Fr, i.e., case F corresponding to Fig. 4(g), the clear one-dimensional horizontal structure (1D-H) is no longer observed but instead some intermediate (1D-HV) one-dimensional structures can be seen for low St values, which converge into a layered curtainlike (2D-L) structure as St is increased. Finally, low values of Fr [case G, Fig. 4(h)] allow the particles to accumulate predominantly in the direction of gravity, so vertical patterns are identified such as 1D-V and 2D-L structures.

D. Clustering pattern variations in relation to constant drift parameter γ

It results from the previous discussion that the variations in inertial and gravity effects do not have a monotonic effect on the particle clustering. Physically, gravity and inertia are combined effects, but one can consider a particle subjected to a drift velocity without referring explicitly to gravity. This effect of drift can be assessed by identifying the patterns with the drift parameter γ instead of Fr. So here we want to observe the variation in the particle attractor by keeping the drift parameter γ constant. Figure 5 shows the three cases $\gamma = 0.135$, 0.689, and 2, as St increases for the arbitrary time $t = 300$. It is not possible to keep the same range for St for all cases because St and γ are linked.

For low values of $0 \leqslant \gamma \leqslant 0.2$ (Fig. 5, top), particles tend to accumulate as a horizontal attractor for low values of St. As observed previously, further increases in St lead to particles scattering. Eventually, particles disperse evenly in the flow for high values of St.

As γ increases, $0.2 \leqslant \gamma \leqslant 0.8$ (Fig. 5, middle), horizontal attractors are no longer observed for low values of St; instead, some intermediate 1D-HV and vertical 1D-V attractors are observed with increasing values of St. Further increases in inertia disperse the particles evenly in the flow field. The third case, $0.8 < \gamma < 2$ (Fig. 5, bottom), corresponds to relatively high values of γ. The particles are trapped in a 2D-L structure. The increase in St results in the particles dispersing more homogeneously on this 2D-L attractor.

To summarize, an increase in γ can lead to a 1D-V or 2D-L rather than a 1D-H attractor, and an increase in St destroys the one-dimensional attractor, leading to the particles reorganizing on a 2D-L.

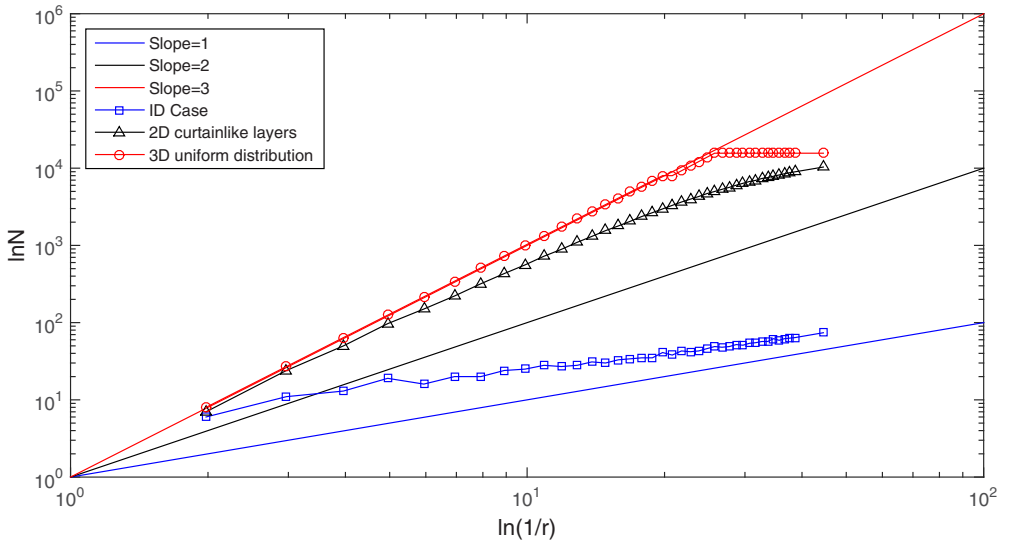

FIG. 6. (Color online) Benchmark for BCM.

This is in agreement with Ref. [8], which mentions gravity-driven clustering of inertial particles in turbulence and reports a different kind of particle clustering caused purely by gravity, that is, clustering in a vertical stripe pattern formed when strong gravity acts on heavy particles.

IV. QUANTIFICATION OF CLUSTERING PATTERNS

Visualizations of the particle cloud for small discrete increments of the nondimensional parameters St and Fr can be tedious. It means looking at about 400 cases in this study in a systematic order. Beyond the simple visualization, it is important to quantify the Lagrangian attractors using an appropriate method for spatial clustering. Two different methods are considered here: the box-counting method (BCM) and the average-distance-to-nearest-neighbor method (Δ). The average-distance-to-nearest-neighbor method is eventually chosen for the final quantitative analysis.

A. Box-counting method

The box-counting method (BCM) is a commonly used method to determine the fractal dimension of an object. Though in our simulation the range of scales is too short to observe the fractal patterns described in [26], BCM remains a useful tool to discriminate between one-dimensional, two-dimensional, and three-dimensional clustering patterns. The fractal dimension D represents the relation between the box size r and the number of boxes N_r needed to cover the cloud of particles, that is,

$$N_r \sim r^D. \tag{19}$$

It is straightforward to obtain the fractal dimension from a log-log plot:

$$D = \frac{\Delta \ln N_r}{\Delta \ln r}. \tag{20}$$

A validation of the method is made on three clearly identified shapes, namely, the one-dimensional Lagrangian attractor,

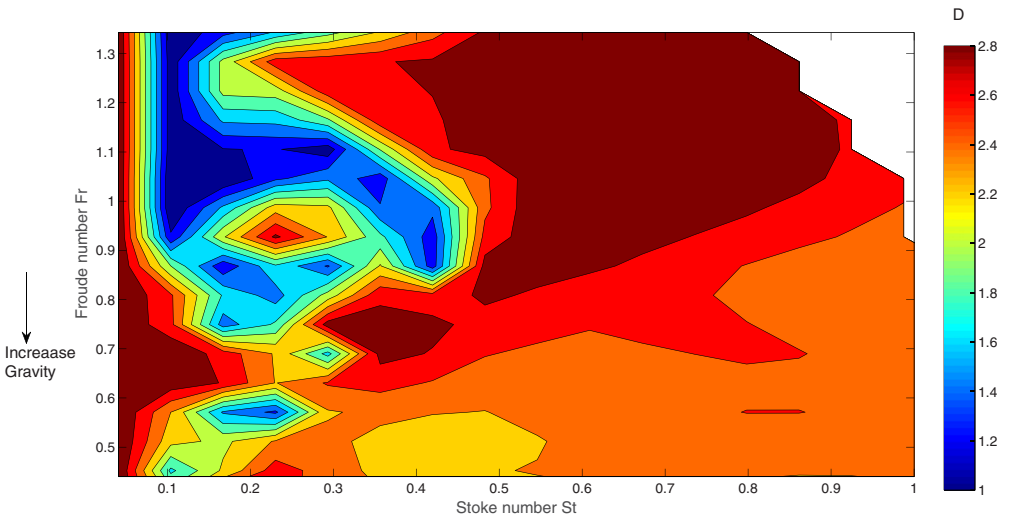

FIG. 7. (Color online) Contour plot of the attractor fractal dimension D as a function of (St, Fr).

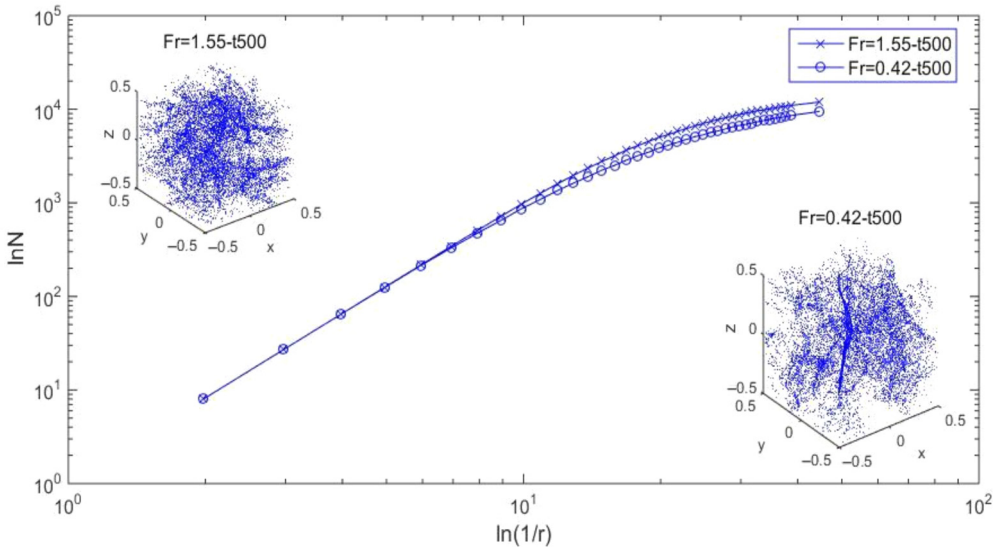

FIG. 8. (Color online) Box-counting slope for very similar cases for different values of Fr at St = 0.207.

the two-dimensional curtainlike layered pattern, and a three-dimensional distribution. As shown in Fig. 6, the difference between these three patterns is clearly captured.

The BCM is sensitive to the achievement of the attractor; that is, if few particles have not settled on the attractor, they can alter the box-counting results. So, with this method, it is necessary to make sure that the cloud shape is the asymptotic final one which requires a very long time. As illustrated in Fig. 2, though at a very short time $t = 10$ the position and shape of the 1D-V is obvious, it is necessary to wait up to $t = 1200$ to get the final cluster position that will allow a correct measure for the BCM. All of the cases are reported in Fig. 7 for clusters having reached their final shapes (attractors). Isocontours of D as a function of (St, Fr) are plotted in Fig. 7 and it appears that for St > 0.45, strong one-dimensional clustering has vanished.

A major problem with the box-counting method is to discriminate between the dimension D of very similar patterns, as shown in Fig. 8. Therefore, we cannot be sure that the box-counting result is meaningful in a case with no clear structures (i.e., without an integer dimension). As mentioned earlier, in order to be accurate, the BCM must be applied to the Lagrangian attractor. If the particle cloud has not settled on the attractor as at time $t = 10$ or $t = 600$ in Fig. 2, the BCM will not educe the 1D patterns. So, in practice, it means running the cases for long times until the particles have all settled on the Lagrangian attractor, which can be prohibitive.

B. Nearest-neighbor-distance analysis

The advantage of using this approach is that it is not necessary to reach the final cluster at $t \to \infty$; a snapshot at earlier times gives us a clear idea of the kind of Lagrangian attractor to expect. For example, in Fig. 2, the kind of 1D-V Lagrangian attractor is clear at $t = 10$ and there is no need to wait for the final asymptotic shape at $t = 1200$. Though other methods may struggle to pick up the structure at $t = 10$ and will only give the correct diagnosis when all of the points have settle on the attractor, that is, for $t = 1200$, the nearest-neighbor-distance analysis will work for intermediary times. The average distance to the nearest neighbor Δ [8] is introduced to systematically quantify the clustering patterns. At a given time for each particle $\mathbf{X}_m$, its nearest neighbor $\mathbf{X}_n$ is such that

$$\Delta_{mi}^2 = (x_m - x_i)^2 + (y_m - y_i)^2 + (z_m - z_i)^2 \qquad (21)$$

is a minimum for $i = n$. Then we define the average distance to the nearest neighbor as

$$\Delta = \frac{1}{N_p}\sqrt{\sum_{m=1}^{N_p} \Delta_{mn}^2}, \qquad (22)$$

where $\mathbf{X}_n = (x_n, y_n, z_n)$ is the nearest particle's neighbor.

We get three obvious benchmark values for this method:

(i) If the particles are homogeneously distributed as at time $t = 0$ [Fig. 1(a)], then $\Delta \simeq L_x/N = 1/25 = 0.04$.

(ii) If the particles are distributed on a surfacelike attractor 2D-L as in Fig. 5, then $\Delta \simeq L_x/N^{3/2} = 1/25^{3/2} = 0.008$.

(iii) If the particles are distributed on a linelike attractor as in Fig. 2, then $\Delta \simeq L_x/N^3 = 1/25^3 = 6.4\,10^{-5}$.

In practice, the method will detect a one-dimensional structure (1D-H or 1-DV) for $\Delta \leqslant 0.008$, while 2D layered structures are observed for $0.01 \leqslant \Delta \leqslant 0.014$.

We applied the average-distance-to-nearest-neighbor method to all run cases to see the variations in the attractor patterns for the same time, $t = 300$. Colorwise, blue (darkest spots for St $\leqslant 0.4$) corresponds to the 1D Lagrangian attractor, yellow-green (light gray) to the 2D-L, and dark red (darkest spots for St $\geqslant 0.4$) to 3D structures. Isocontours of Δ are plotted as functions of (St, Fr) in Fig. 9(a) and (St, γ) in Fig. 9(b) to see the effect of varying gravity and inertia on the Lagrangian attractors. Figure 9 confirms that the clustering of inertial particles is not a monotonic function of either St or Fr number. However, it is possible to identify regions in the plane (St, Fr):

(i) In agreement with Fig. 7, there are no one-dimensional structures for St $\geqslant 0.5$.

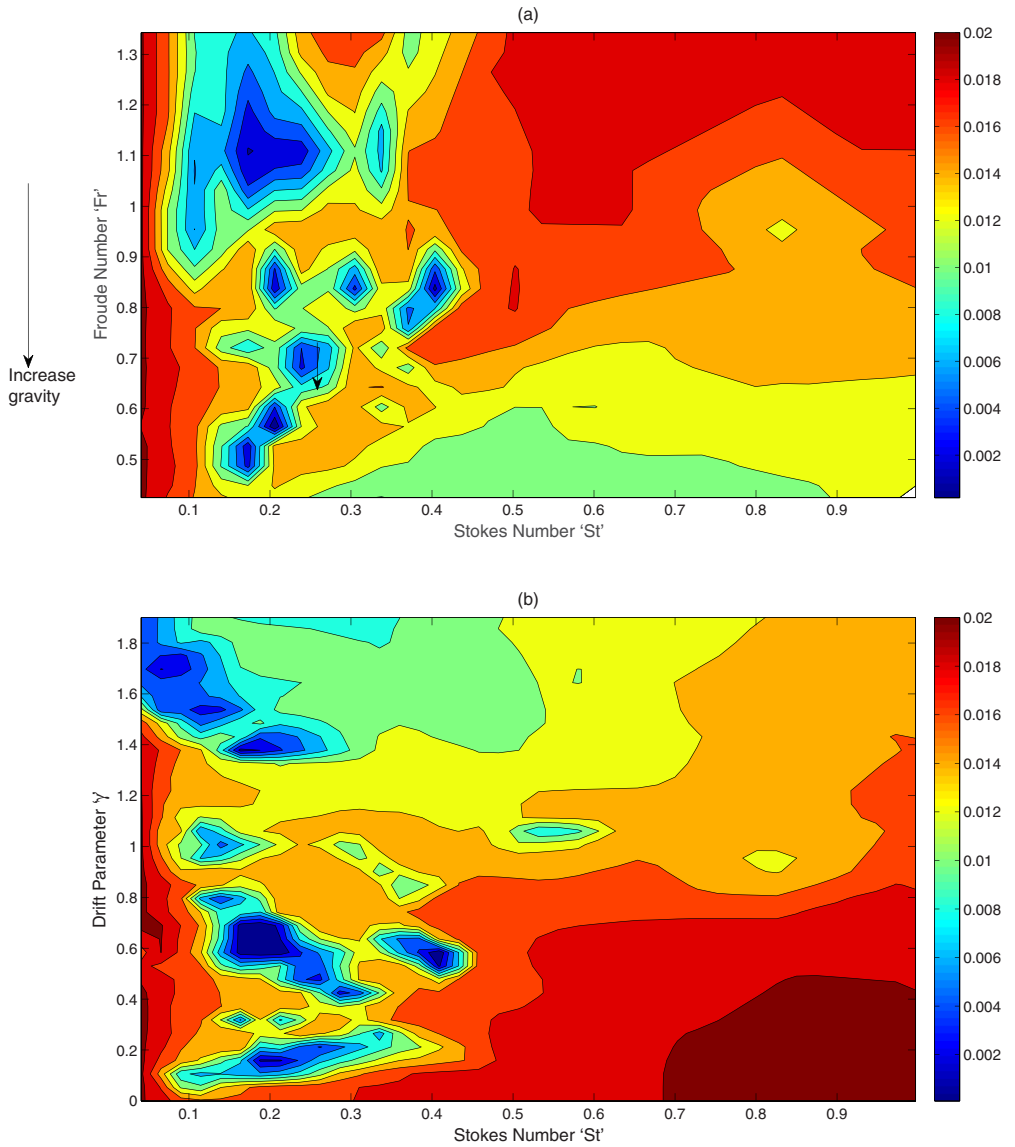

FIG. 9. (Color online) Isocontours of (a) Δ(St,Fr) and (b) $\Delta(\mathrm{St},\gamma)$ showing different types of clusterings.

(ii) We can refine the analysis in term of γ: In Fig. 9(b), for large values of the Stokes number (St $>$ 0.3) and gravity effects ($\gamma > 0.8$), the 2D-L structures are predominant. This is also in agreement with [9], whose calculations show that for large values of St, particles may cluster strongly.

Another advantage of the average-distance-to-nearest-neighbor method is that variations in horizontal Δ_H and vertical Δ_V directions can be identified separately, which helps to monitor anisotropic patterns. In practice, Δ_H and Δ_V are defined as follows:

$$\Delta_H = \frac{1}{N_p}\sqrt{\sum_{m=1}^{N_p}(x_m - x_n)^2 + (y_m - y_n)^2}, \qquad (23)$$

$$\Delta_V = \frac{1}{N_p}\sqrt{\sum_{m=1}^{N_p}(z_m - z_n)^2}. \qquad (24)$$

Figure 10(a) shows the isocontours of Δ as a function of (St, Fr) in the region where one-dimensional Lagrangian attractors are observed, i.e., $0.05 \leqslant \mathrm{St} \leqslant 0.4$. The two different types of one-dimensional attractor, either horizontal (1D-H) or vertical (1D-V), are further analyzed in Figs. 10(b) and 10(c). Figure 10(c) shows the ratio Δ_H/Δ where one-dimensional attractors exist, that is, when $\Delta \leqslant 0.008$. $\Delta_H/\Delta \leqslant 0.5$, which are the blue points (light gray area), indicate 1D-V structures; whereas $\Delta_H/\Delta \geqslant 0.75$, which are the red points (dark spots for Fr $\geqslant 0.7$), indicate 1D-H structures. Figure 10(b) describes a similar relationship based on Δ_V. So it is clear from the points' color distribution that horizontal attractors are predominant for large Fr, while vertical attractors are prevalent as Fr decreases.

V. CONCLUSION

We used kinematic simulation (KS) to study the clustering pattern of particles with inertia subjected to gravity effects. For some combined inertia and gravity effects (St, Fr), the particles cluster on a fixed space subset. That subset can be one dimensional or two dimensional. In most of the

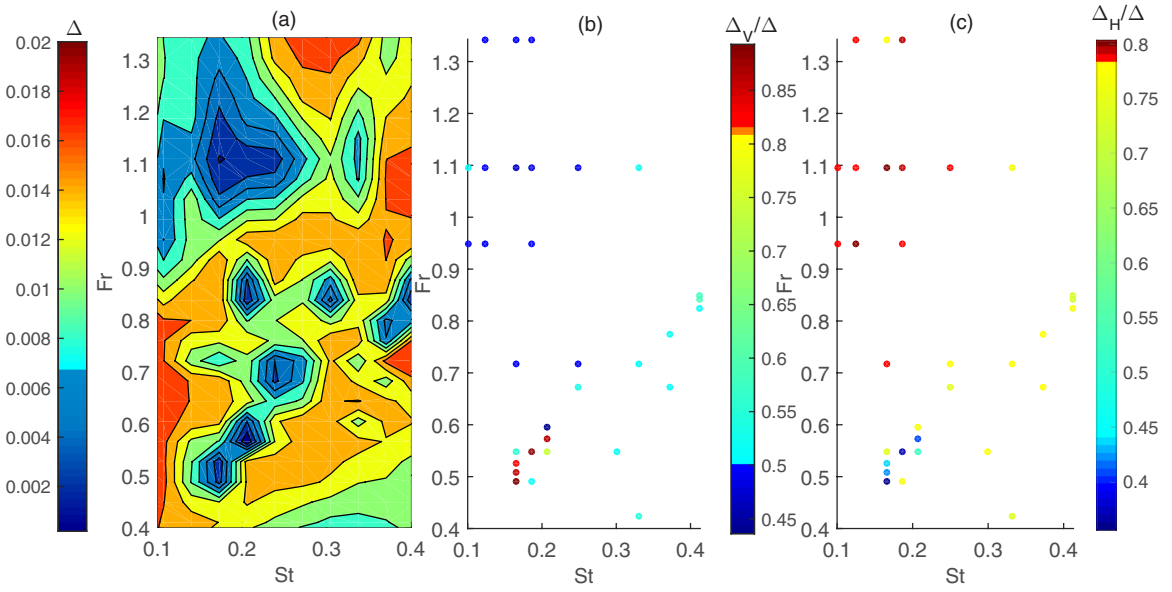

FIG. 10. (Color online) (a) Iso-contours of Δ as a function of (St, Fr), (b) Δ_V/Δ when $\Delta \leqslant 0.006$, c) Δ_H/Δ when $\Delta \leqslant 0.006$.

cases, the particles did not cluster and disperse, occupying most of the periodic box.

Using KS, it became possible to investigate many combinations of (St, Fr) and educe and classify those one-dimensional or two-dimensional subsets. Though KS retains only part of the turbulence physics, it helps to understand the clustering patterns and the effect of gravity on these patterns.

The main results can be summarized as follows (and in a more synthetic presentation in Fig. 11):

(a) The effect of gravity may reduce or enhance inertial particles clustering (as noticed in [9,10]) depending on the Stokes number. This effect can lead to strongly anisotropic clusterings (1D or 2D-L), which are very clearly evidenced by the KS model.

(b) The 1D structure is better observed with the synthetic flow, as in real flows unsteadiness may prevent the particles from reaching that asymptotic state. These 1D attractors move from the horizontal to the vertical direction as the Fr number decreases.

(c) For our range of Froude numbers, we found two critical Stokes numbers: for $\mathrm{St} > \mathrm{St}_{cr1} = 0.3$ there is never occurrence of a horizontal (1D-H) type attractor, and no 1D-type attractor is found for $\mathrm{St} > \mathrm{St}_{cr2} = 0.5$.

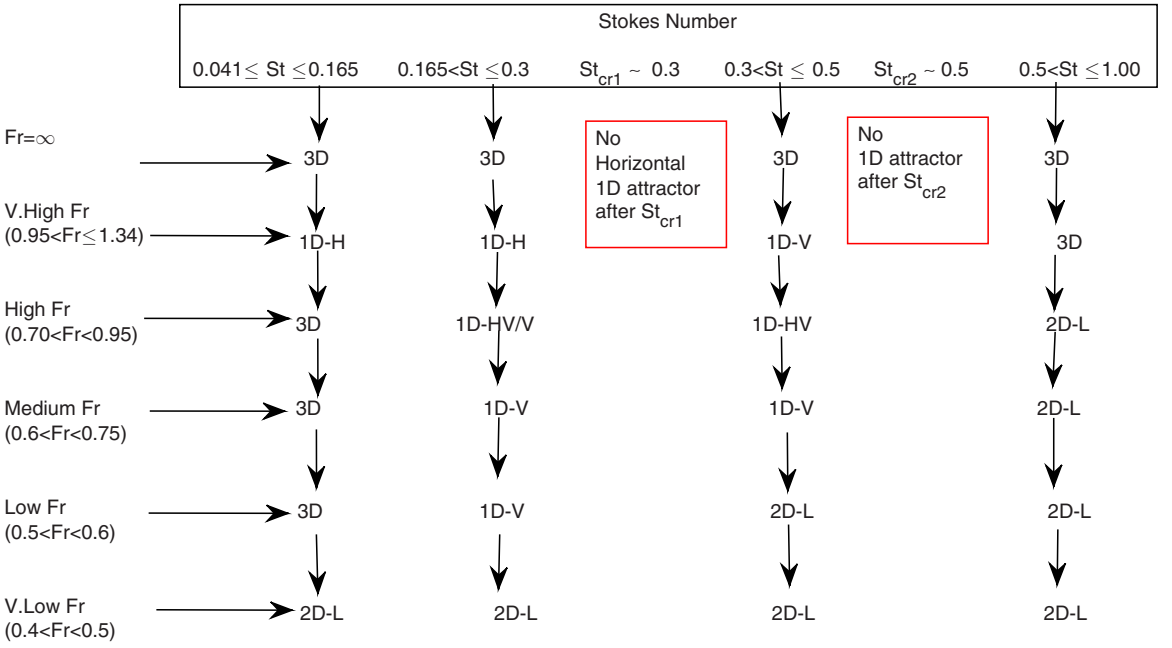

FIG. 11. (Color online) Flow chart describing the different attractors in relation to the two critical values of St.

(d) For low values of Fr, curtainlike two-dimensional layered structures similar to the "curtainlike manifolds" already observed in [7] are recovered as the high gravity prevents the inertial particles from settling uniformly in the turbulent flow.

ACKNOWLEDGMENTS

M.F. gratefully acknowledges financial support from the Department of Mechanical Engineering of the University of Engineering and Technology Lahore, Pakistan. This work was supported by EPSRC Grant No. EP/L000261/1.

[1] G. Falkovich, A. Fouxon, and M. G. Stepanov, Nature (London) **419**, 151 (2002).
[2] L. Pan, P. Padoan, J. Scalo, A. G. Kritsuk, and M. L. Norman, Astrophys. J. **740**, 6 (2011).
[3] M. Cencini, J. Bec, L. Biferale, G. Boffetta, A. Celani, A. Lanotte, S. Musacchio, and F. Toschi, J. Turbulence **7**, 36 (2006).
[4] E. W. Saw, J. P. L. C. Salazar, L. R. Collins, and R. A. Shaw, New J. Phys. **14**, 105030 (2012).
[5] G. Falkovich and A. Pumir, Phys. Fluids **16**, L47 (2004).
[6] J. Bec, L. Biferale, M. Cencini, A. Lanotte, S. Musacchio, and F. Toschi, Phys. Rev. Lett. **98**, 084502 (2007).
[7] E. J. P. Woittiez, H. J. J. Jonker, and L. M. Portela, J. Atmospher. Sci. **66**, 1926 (2008).
[8] Y. Park and C. Lee, Phys. Rev. E **89**, 061004(R) (2014).
[9] K. Gustavsson, S. Vajedi, and B. Mehlig, Phys. Rev. Lett. **112**, 214501 (2014).
[10] J. Bec, H. Homann, and S. S. Ray, Phys. Rev. Lett. **112**, 184501 (2014).
[11] J. Fung, J. Hunt, N. Malik, and R. Perkins, J. Fluid Mech. **236**, 281 (1992).
[12] F. W. Elliott and A. J. Majda, Phys. Fluids **8**, 1052 (1996).
[13] N. A. Malik and J. C. Vassilicos, Phys. Fluids **11**, 1572 (1999).
[14] F. Nicolleau and G. Yu, Phys. Rev. E **76**, 066302 (2007).
[15] F. C. G. A Nicolleau and A. F. Nowakowski, Phys. Rev. E **83**, 056317 (2011).
[16] N. A. Malik, arXiv:1405.3625.
[17] N. A. Malik, arXiv:1405.3638.
[18] F. Nicolleau, K.-S. Sung, and J. Vassilicos, Flow Turbulence Comb. **91**, 79 (2013).
[19] R. H. A. Ijzermans, E. Meneguz, and M. W. Reek, J. Fluid Mech. **653**, 99 (2010).
[20] E. Meneguz and M. W. Reeks, J. Fluid Mech. **686**, 338 (2011).
[21] J. C. H. Fung and J. C. Vassilicos, Phys. Rev. E **57**, 1677 (1998).
[22] F. Nicolleau and A. ElMaihy, Phys. Rev. E **74**, 046302 (2006).
[23] A. Abou El-Azm Aly and F. Nicolleau, Phys. Rev. E **78**, 016310 (2008).
[24] R. Gatignol, J. Mech. Theor. Appl. **1**, 143 (1983).
[25] M. R. Maxey and J. J. Riley, Phys. Fluids **26**, 883 (1983).
[26] F. Nicolleau and A. ElMaihy, J. Fluid Mech. **517**, 229 (2004).